International Journal of Mathematics and
Computer Science, **17**(2022), no. 2, 695–709

A study of a Hamiltonian system with potential surface energy posses one channel and two potential wells

Ashwaq Almohaimeed, Ali Allahem

Department of Mathematics
College of Science
Qassim University
Buraydah, Saudi Arabia

email: aallahem@qu.edu.sa

(Received October 8, 2021, Accepted November 15, 2021)

Abstract

In this paper, we present the results of a preliminary analytical and numerical study of a dynamical system with potential surface energy possessing one channel and two potential wells. The time series for the system can be derived and represented for three sensitive cases indicating the dynamic behaviors.

1 Introduction

A theoretical understanding of the underlying processes that govern selectivity or product distributions is an important component of an organic chemical reaction study. Previous research [1, 2, 3, 4, 5, 6, 7, 8, 9] on the subject has often revolved around a potential energy surface (PES) with two consecutive index-1 saddles and no energy minimum in between. The response starts when a trajectory passes the higher-energy saddle and approaches the lower-energy saddle, known as the entry channel. Product selectivity is the issue of which the trajectory enters in this channel containing two wells on each side.

Key words and phrases: Hamiltonian, Potential energy surface, Stability, Time Series and Chaos.
AMS (MOS) Subject Classifications: 00A05, 11S82, 15A06 15A60, 30C30.
ISSN 1814-0432, 2022, http://ijmcs.future-in-tech.net

Our work varies from others [10] in two respects. First, we consider the two wells in the PES to be symmetric. Secondly the phase space structures control selectivity with respect to the geometric structures that emerge from the UPOs and control access to the entrance channel and thus the two wells are well defined. The symmetric of PES provides product distribution information which helps to understand how phase space structures direct selectivity.

2 The Hamiltonian Model

Collins et al. [10] considered a reduced form of their work due to the symmetry of PES along the x-axis. Because the researchers want to know the underlying phase space process governing selectivity in this class of energy landscapes with a 1:1 product ratio resulting from trajectories branching, this assumption is made [11]. The exit/entrance channel, an energy barrier that divides two potential wells and is characterized by two index-1 saddles (upper and lower), is a critical part of the topography in our PES. Figure 1 illustrates the PES's topographic characteristics and equipotential map. The index-1 saddles (upper and lower) have been referred to as red diamonds while the minima of the potential wells with red dots. The blue arrows indicate that there is a potential of pathways for trajectories entering the system through the upper channel, illustrating the chemical selectivity mechanism [11].

The potential energy surface that we are studying, has two index-1 saddles transition state (TS) at a certain level of energy. One index-1 form one of two products. The other index-1 saddle is a ridge with lower energy which is a TS for the isomerization reaction interconverting the two products [10].

Consider a system with two degrees of freedom (DoF) with given coordinates (x, y) [10]. The potential energy function is a modified version of a model potential of Carpenter [12]:

$$\begin{aligned} V(x,y) = c_0\left(\frac{1}{3}x^3 - \frac{1}{2}\alpha x^2\right) + \frac{1}{2}\omega^2 y^2(1-\beta x) + c_1 y^4 x + c_2 x^2 y^2 \\ + c_3 y x^2 + c_4 x y^2 + c_5 x y + c_6 x y^3, \end{aligned} \tag{2.1}$$

Two parameters are fixed at $\alpha = 2$, $\beta = 2$, $c_0 = 3$, $\omega = \sqrt{3}$ and the remaining six, c_k, where $k = 1, \ldots, 6$, are determined by finding the locations and energies of the minima of the upper and lower wells. In other words, by solving a set of linear equations [10].

The upper index-1 saddle point is located at the origin $(0,0)$ with energy $V_0 = 0$, and the lower index-1 saddle point is located at $(1,0)$ with energy $V_0 = -4/3$. On the other hand, the potential wells are fixed at $(x,y) = (1.107146, -0.879883)$ with energy level $V = -1.94773$ which is so-called the potential well (bottom) where $y < 0$ and at $(x,y) = (1.107146, 0.879883)$ with energy level $V = -1.94773$ which is so-called the potential well (top) where $y > 0$ [11].

The Hessian H is the matrix of second-order partial derivatives:

$$H(x,y) = \begin{pmatrix} V_{xx} & V_{xy} \\ \\ V_{yx} & V_{yy} \end{pmatrix},$$

where subscripts show partial differentiation [10]. In our model, the mass tensor/kinetic energy $m_x = m_y = 1$ is negligible. The covariant derivatives of the potential do not need to be considered in the case of a Hamiltonian with coordinate-dependent kinetic energy[13].

Using a Hamiltonian based on the two potential equation, we investigated reaction dynamics (2.1). As a result, the dynamics were studied on a short enough timescale to rule out energy transfer to or from other DoFs. Nevertheless, dissipation was included in the model to account for the impact of additional DoFs. These additional degrees of freedom were not included in this study. However, they will be studied in the near future. We refer the reader to the useful resources [14, 15, 16, 17, 18, 19, 20, 21, 22, 23].

The total of kinetic and potential energy is expressed with the following form in the two DoF Hamiltonian model [10]:

$$H(x,y,p_x,p_y) = \frac{p_x^2}{2m_x} + \frac{p_y^2}{2m_y} + V(x,y),$$

where the potential $V(x,y)$ in equation (2.1)

$$V(x,y) = \frac{8}{3}x^3 - 4x^2 + \frac{1}{2}y^2 + xy^2\left(y^2 - 2\right), \tag{2.2}$$

Hamilton's equations of motion are:

$$\begin{cases} \dot{x} = p_x, \\ \dot{y} = p_y, \\ \dot{p}_x = -\dfrac{\partial V}{\partial x}(x,y), \\ \dot{p}_y = -\dfrac{\partial V}{\partial y}(x,y). \end{cases}$$

where the x mass is denoted by m_x and the y mass is denoted by m_y DoF respectively $m_x = m_y = 1$. Thus, the Hamilton's equations of motion become:

$$\begin{cases} \dot{x} = \dfrac{\partial H}{\partial p_x} = p_x, \\ \dot{y} = \dfrac{\partial H}{\partial p_y} = p_y, \\ \dot{p}_x = -\dfrac{\partial H}{\partial x} = 8x(1-x) + y^2(2-y^2), \\ \dot{p}_y = -\dfrac{\partial H}{\partial y} = y\left[4x(1-y^2) - 1\right]. \end{cases} \tag{2.3}$$

$$\dot{p}_x = -\frac{\partial H}{\partial x} = 8x(1-x) + y^2\left(2-y^2\right) = 8x - 8x^2 + 2y^2 - y^4, \tag{2.4}$$

$$\dot{p}_y = -\frac{\partial H}{\partial y} = y\left[4x\left(1-y^2\right) - 1\right] = -4xy^3 + 4xy - y. \tag{2.5}$$

By integrating equation (2.4) in relation to (x), we get

$$H = \frac{8}{3}x^3 - 4x^2 - 2xy^2 + xy^4 + g(y). \tag{2.6}$$

Also, by integrating equation (2.5) in relation to (y), we get

$$H = xy^4 - 2xy^2 + \frac{1}{2}y^2 + f(x). \tag{2.7}$$

From equations (2.7) and (2.6), we get

$$H = xy^4 - 2xy^2 + \frac{8}{3}x^3 - 4x^2 + \frac{1}{2}y^2.$$

$$H = xy^4 - 2xy^2 + \frac{1}{2}y^2 + \phi(x).$$

3 Preliminary results

The fixed points associated with the Hamiltonian system (2.3) can be obtained by setting the right hand sides to zero. Hence, we get

$$\dot{x} = \frac{\partial H}{\partial p_x} = p_x = 0$$

$$\dot{y} = \frac{\partial H}{\partial p_y} = p_y = 0$$

Thus, we have the first fixed point, $(x, y) = (0, 0)$. Also,

$$\dot{p}_y = -\frac{\partial H}{\partial y} = y\left[4x\left(1 - y^2\right) - 1\right] = 0$$

$$-4xy^3 + 4xy - y = 0$$

Thus, we have

$$y = 0 \quad or \quad -y = \pm\sqrt{1 - \frac{1}{4x}}.$$

Also,

$$\dot{p}_x = -\frac{\partial H}{\partial x} = 8x\left(1 - x\right) + y^2\left(2 - y^2\right) = 0$$

$$8x - 8x^2 + 2y^2 - y^4 = 0$$

For $y = 0$, we now have two fixed points

$$(0, 0), (1, 0)$$

Also, for $y = \pm\sqrt{1 - \frac{1}{4x}}$, we have

$$8x - 8x^2 + \left(1 - \frac{1}{4x}\right)\left(1 + \frac{1}{4x}\right) = 0$$

Thus,

$$8x - 8x^2 + \left(1 - \frac{1}{16x^2}\right) = 0$$

Consequently,

$$x \approx 1.107146\ ,\ 0.17111$$

Hence,

$$y = \pm\ 0.879883,$$

As result, we have additional two fixed points

$$(1.107146, 0.879883)\,, (1.107146, -0.879883)\,.$$

The fixed points that result are as follows:

$$(0,0)\,, (1,0)\,, (1.107146, 0.879883)\,, (1.107146, -0.879883) \tag{3.8}$$

The potential energy value associated with the Hamiltonian system at the fixed points (3.8) can be obtained by substituting in potential function (2.2). Thus, we have energy values that are equal $0, -\frac{4}{3}, -1.94773$ and -1.94773 for the fixed points in (3.8), respectively.

Using the Hessian matrices,

$$H(x,y) = \begin{pmatrix} \dfrac{\partial^2 V(x,y)}{\partial x^2} & \dfrac{\partial^2 V(x,y)}{\partial x \partial y} \\ \dfrac{\partial^2 V(x,y)}{\partial y \partial x} & \dfrac{\partial^2 V(x,y)}{\partial y^2}, \end{pmatrix}$$

$$= \begin{pmatrix} 16x - 8 & 4y^3 - 4y \\ 4y^3 - 4y & 12xy^2 - 4x + 1 \end{pmatrix}$$

1. $H(0,0) = \begin{pmatrix} -8 & 0 \\ 0 & 1 \end{pmatrix}$

$$P(\lambda) = \lambda^2 + 7\lambda - 8.$$

The eigenvalues are

$$\lambda_1 = 1 > 0, \quad \lambda_2 = -8 < 0.$$

Therefore, stability takes the form of saddle and then, $V(x,y)$ has a saddle point at $(0,0)$.

2. $H(1,0) = \begin{pmatrix} 8 & 0 \\ 0 & -3 \end{pmatrix}$

$$P(\lambda) = \lambda^2 - 5\lambda - 24.$$

The eigenvalues are

$$\lambda_1 = 8 > 0, \quad \lambda_2 = -3 < 0.$$

Therefore, stability takes the form of saddle and then, $V(x, y)$ has a saddle point at $(1, 0)$.

3. $H(1.107146, 0.879883) = \begin{pmatrix} 9.714336 & -0.794731 \\ -0.794731 & 6.857166 \end{pmatrix}$

$$P(\lambda) = \lambda^2 - 16.571502\lambda + 65.981217.$$

The eigenvalues are

$$\lambda_1 = 9.920514 > 0, \quad \lambda_2 = 6.650987 > 0.$$

Therefore, stability takes the form of unstable node and then, $V(x, y)$ has a local minimum value at $(1.107146, 0.879883)$.

4. $H(1.107146, -0.879883) = \begin{pmatrix} 9.714336 & 0.794731 \\ 0.794731 & 6.857166 \end{pmatrix}$

$$P(\lambda) = \lambda^2 - 16.571502\lambda + 65.981217.$$

The eigenvalues are

$$\lambda_1 = 9.920514 > 0, \quad \lambda_2 = 6.650987 > 0.$$

Therefore, stability takes the form of unstable node and then, $V(x, y)$ has a local minimum value at $(1.107146, -0.879883)$.

4 Numerical Results and Discussion

In this paper, the phase space mechanisms that govern selectivity were introduced in such a way that individual reaction paths could be predicted. The Hamiltonian system (2.3) was solved numerically with the initial conditions (x, y) and time t. For $0 \leq t \leq t_{max} = 100$ time units, similar to the natural period for motion in each well, trajectories are integrated. The ratio of well-occupancies has kept far from an asymptotic value (steady-state) even at $t = t_{max}$, showing that nontrivial isomerization dynamics are still occurring. However, in our calculations, these oscillations could be due to the finite size

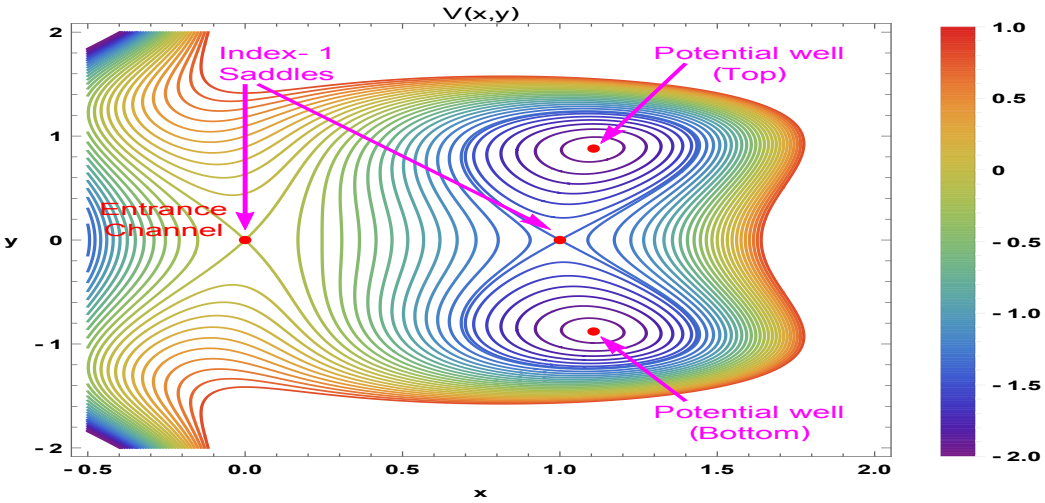

Figure 1: The description of equipotential contours of the PES can be found in equation (2.2).

of the trajectory group. The initial conditions include an initial time, a set of mathematical equations or a physical system emerges from this time. As a result, the resolution can be set to represent a satisfactory or unique maximal solution to the same end. Initial conditions are divided into three categories: A, B, and C, namely $(x_0 = 0.1, y_0 = 0.26)$ for A, $(x_0 = 0.09, y_0 = 0.28)$ for B and $(x_0 = 0.09, y_0 = -0.28)$.

A fourth-order Runge-Kutta method with appropriate time stepping was used to integrate the system (2.3). The solutions were integrated over a number of oscillations to ensure that a stable final state was achieved. Numerical integrations for cases A, B, and C always converged to the steady solution given by (3.8). The solutions have a regular structure (See Figures 2,3,4), even if they are not periodic. Figure 2 shows four representations of the numerical solution for finite time $(t, 0, 100)$. In other words, time series were shown for the x, y, p_x and p_y coordinates, respectively. Similarly, Figure 3 shows four representations of the numerical solution for finite time $(t, 0, 100)$ that travel to the top well. In other words, time series were shown for the x, y, p_x and p_y coordinates, respectively. Finally, Figure 4 shows four representations of the numerical solution for finite time $(t, 0, 100)$ that travel to the bottom well. That is, time series were shown for the x, y, p_x and p_y coordinates, respectively. Choosing the initial conditions between A and B is sensitive because some initial conditions will travel to the top well while others will travel to the bottom well.

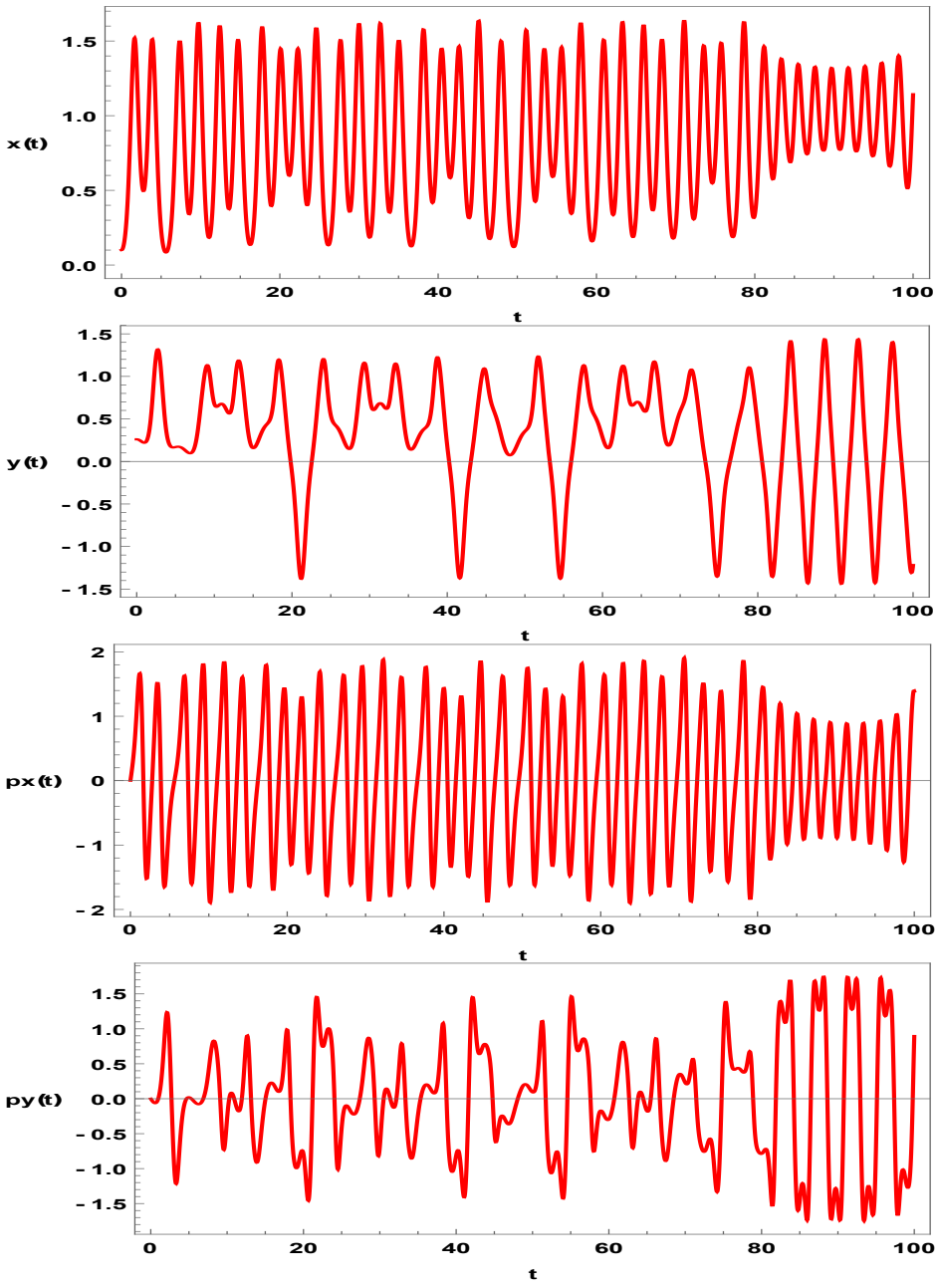

Figure 2: Plot of equation motions with initial condition $(x_0 = 0.1, y_0 = 0.26)$ and time $(t, 0, 100)$.

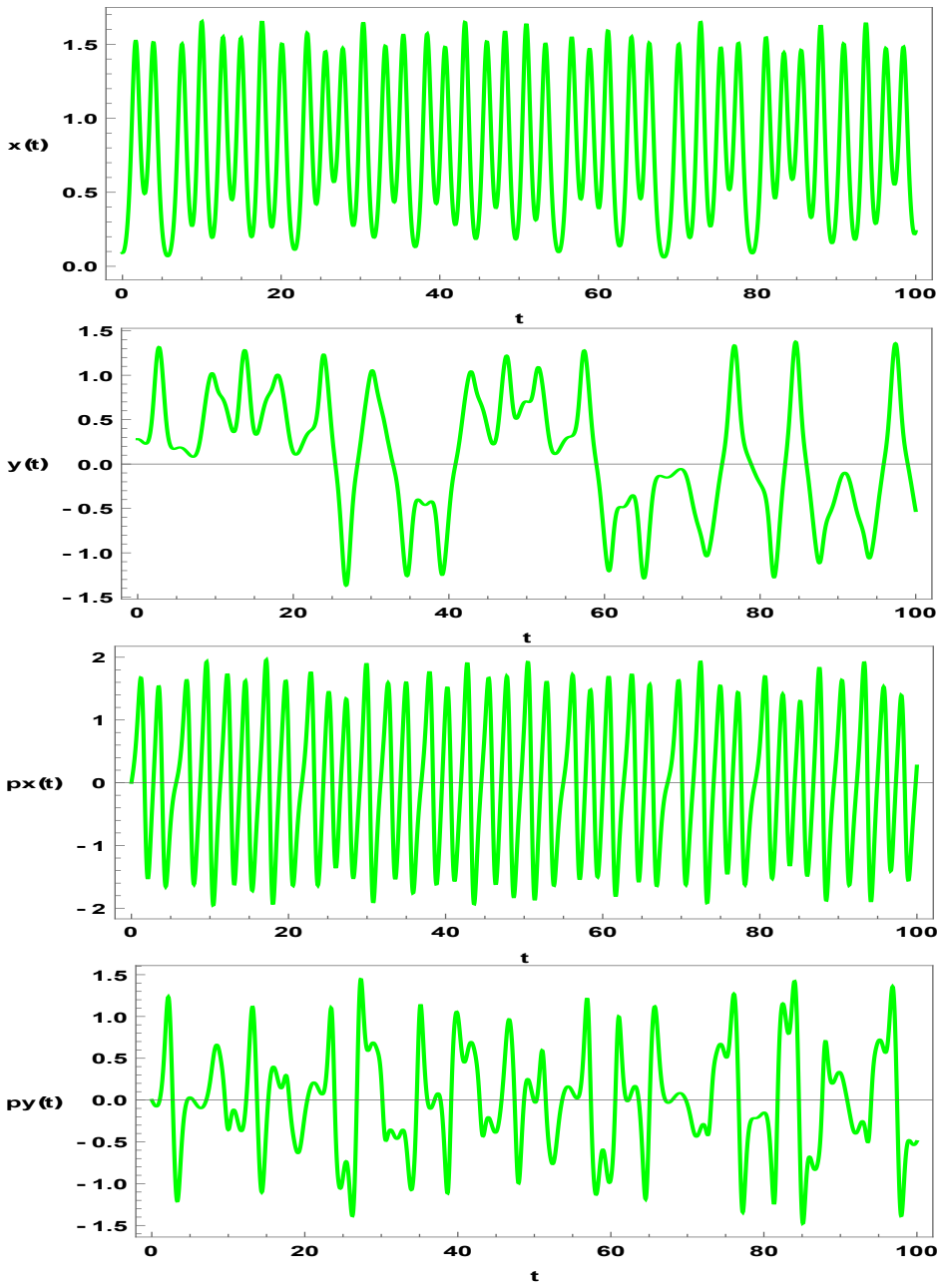

Figure 3: Plot of equation motions with initial condition $(x_0 = 0.09, y_0 = 0.28)$ and time $(t, 0, 100)$.

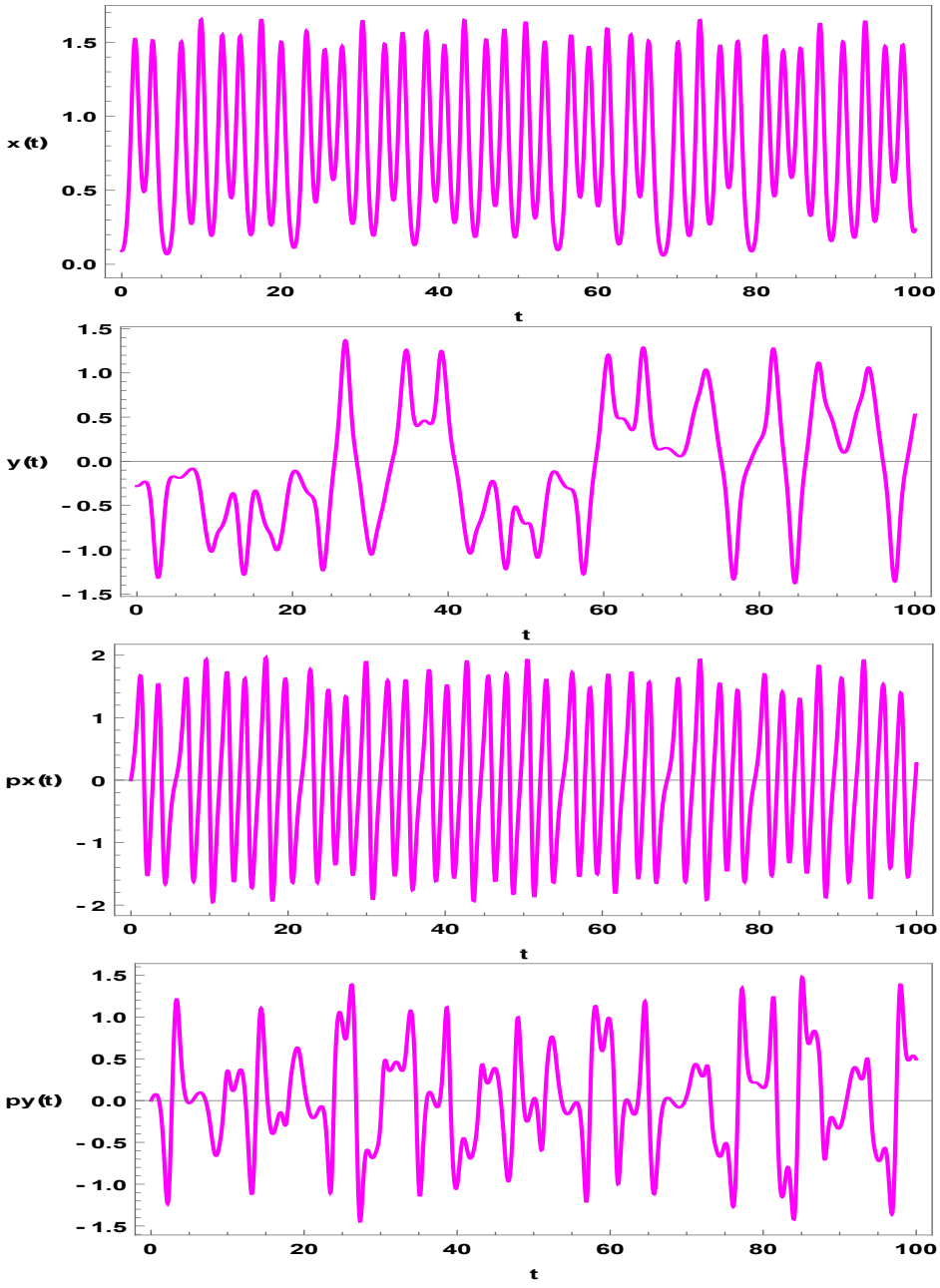

Figure 4: Plot of equation motions with initial condition $(x_0 = 0.09, y_0 = -0.28)$ and time $(t, 0, 100)$.

In figure 5, the reactive trajectory (red) starts at the entrance region, travels to the energy barrier, and then returns to the exit region, never stopping at either well. The reacting trajectory (green, pink) starts at the entrance and travels to the top or bottom of the well. The UPOs of the upper index-1 saddle, the top well (top UPO), and the bottom well (bottom UPO) are represented by the three blue curves (bottom UPO). The top index-1 saddle's UPO manages entry and exit from the reaction region, while the other two UPOs manage entry and exit from their respective wells via the UPOs' stable and unstable manifolds. $UPOs$ in two DoF Hamiltonian systems include $2D$ manifolds (stable and unstable) on $3D$ energy surface. They divide this surface due to their dimensionality and are unable to pass through it due to their invariance. As a result, they constitute barriers to phase space transport, limiting how trajectories evolve in phase space.

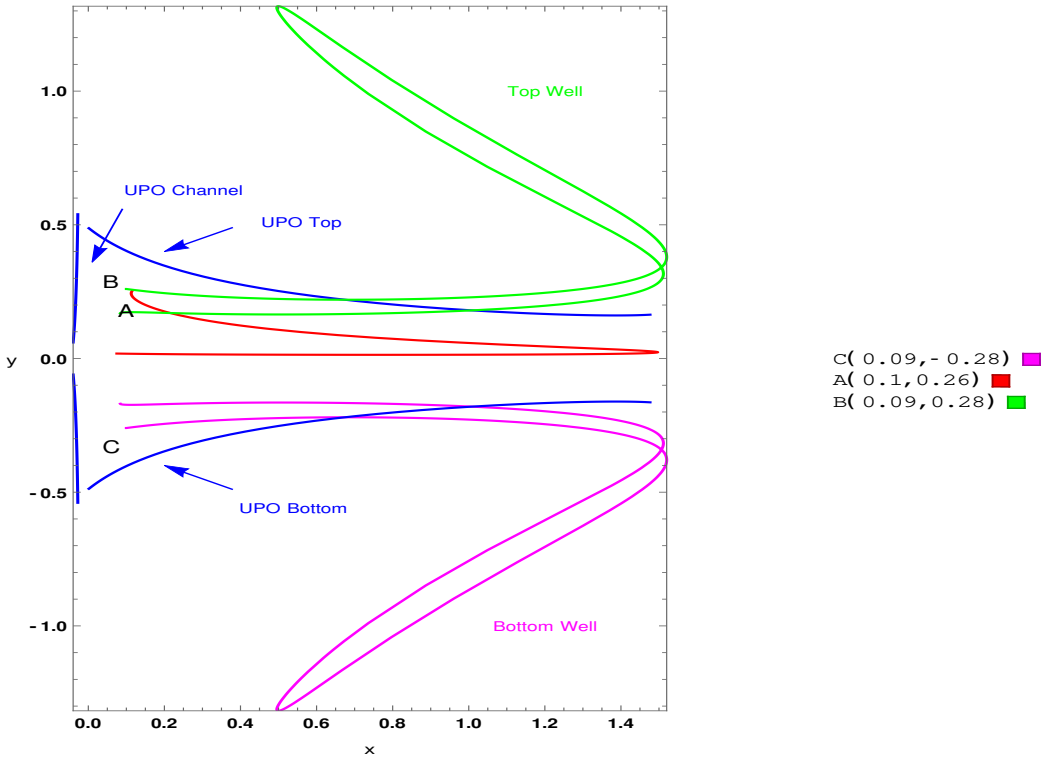

Figure 5: Phase space structure and forward time evolution of trajectories in qualitative analysis of system dynamics and evolution of corresponding trajectories projected onto configuration space.

5 Conclusion

The system with potential surface energy posses one channel and two potential wells is valuable and many cases can be studied to see the beauty of the dynamical system including, Chaos, Bifurcations and periodic orbits. In our case, we showed how time series for the system can be derived and represented. Also, we showed the sensitivity of the initial conditions can decide the direction of trajectories to either top or bottom well. A chaos case has been noticed which can be studied in future work. The Lyapunov exponent tool [24] has a great potential to measure the divergence in the chaotic cases.

Acknowledgment. The authors would like to thank the Mathematics Department at Qassim University in Saudi Arabia.

References

[1] Julia Rehbein, Barry K. Carpenter, Do we fully understand what controls chemical selectivity?, Physical Chemistry Chemical Physics, **47,** (2011), 20906–20922.

[2] Stephanie R. Hare, Dean J. Tantillo, Post-transition state bifurcations gain momentumcurrent state of the field, Pure and Applied Chemistry, **89,** no. 6, (2017), 679–698.

[3] Daniel H. Ess, Steven E. Wheeler, Robert G. Iafe, Lai Xu, Nihan Celebi-Oelcuem, Kendall N. Houk, Bifurcations on potential energy surfaces of organic reactions, Angewandte Chemie International Edition, **47,** no. 40, (2008), 7592–7601.

[4] Abdelbaki Choucha, Salah Mahmoud Boulaaras, Djamel Ouchenane, Ali Allahem, Global existence for two singular one-dimensional nonlinear viscoelastic equations with respect to distributed delay term, Journal of Function Spaces, (2021).

[5] Ali Allahem, Analytical solution to normal forms of Hamiltonian systems, Mathematical and Computational Applications **22,** no. 3, (2017), 37.

[6] Sadok Otmani, Salah Boulaaras, Ali Allahem, The Maximum Norm Analysis of a Nonmatching Grids Method for a Class of Parabolic $p(x)$-

Laplacian Equation, Boletim Sociedade Paranaense de Matemática, (2019).

[7] Ali Allahem, New derived systems of Hide's coupled dynamo model, European Journal of Pure and Applied Mathematics, **10,** no. 4, (2017), 858–870.

[8] Ali Allahem, Synchronized Chaos of a Three-Dimensional System with Quadratic Terms, Mathematical Problems in Engineering, (2020).

[9] Salah Boulaaras, Ali Allahem, Two-dimensional mathematical model of the transport equations of some pollutants and their diffusion in a particular fluid, Journal of Intelligent and Fuzzy Systems, **38,** no. 3, (2020), 2457–2467.

[10] Pete Collins, Barry K. Carpenter, Gregory S. Ezra, Stephen Wiggins, Nonstatistical dynamics on potentials exhibiting reaction path bifurcations and valley-ridge inflection points, The Journal of chemical physics, **139,** no. 15, (2013), 154108.

[11] M. Agaogrlou, V. J. García-Garrido, M. Katsanikas, S. Wiggins, The phase space mechanism for selectivity in a symmetric potential energy surface with a post-transition-state bifurcation, Chemical Physics Letters, **754,** (2020), 137610.

[12] Barry K. Carpenter, Potential energy surfaces and reaction dynamics Reactive Intermediate Chemistry (R. A. Moss, M. S. Platz, M. Jones Jr., editors), (2004), 925–960.

[13] Akitomo Tachibana, Extended hessian matrix along the reaction coordinate, Theoretica chimica acta, **58,** no. 4, (1981), 301–308.

[14] Petros Valtazanos, Klaus Ruedenberg, Bifurcations and transition states, Theoretica chimica acta, **69,** no. 4, (1986), 281–307.

[15] David Martin Birney, Theory, experiment and unusual features of potential energy surfaces of pericyclic and pseudopericyclic reactions with sequential transition structures, Current Organic Chemistry, **14,** no. 15, (2010), 1658–1668.

[16] Wolfgang Quapp, How does a reaction path branching take place? A classification of bifurcation events, Journal of molecular structure, **695,** (2004), 95–101.

[17] Daniel A. Singleton, Chao Hang, Michael J. Szymanski, Matthew P. Meyer, Andrew G. Leach, Keith T. Kuwata, Jenny S. Chen, Alexander Greer, Christopher S. Foote, K. N. Houk, Mechanism of ene reactions of singlet oxygen. A two-step no-intermediate mechanism, Journal of the American Chemical Society, **125,** no. 5, (2003), 1319–1328.

[18] M. Agaoglou, B. Aguilar-Sanjuan, V. J. García-Garrido, R. García-Meseguer, F. González-Montoya, M. Katsanikas, V. Krajňák, S. H. Naik, S. Wiggins, Chemical reactions: A journey into phase space, Zenodo, **1,** (2019).

[19] J. A. Jiménez Madrid, Ana M. Mancho, Distinguished trajectories in time dependent vector fields, Chaos: An Interdisciplinary Journal of Nonlinear Science, **19,** no. 1, (2009), 013111.

[20] Carlos Lopesino, Francisco Balibrea-Iniesta, Vctor J. García-Garrido, Stephen Wiggins, Ana M. Mancho, A theoretical framework for Lagrangian descriptors, International Journal of Bifurcation and Chaos, **27,** no. 1, (2017), 1730001.

[21] Ana M. Mancho, Stephen Wiggins, Jezabel Curbelo, Carolina Mendoza, Lagrangian descriptors: A method for revealing phase space structures of general time dependent dynamical systems, Communications in Nonlinear Science and Numerical Simulation, **18,** no. 12, (2013), 3530-3557.

[22] Peter Bönzli, Albin Otter, Markus Neuenschwander, Hanspeter Huber, Hans Peter Kellerhals, 1H- and 13C-NMR Investigation of Pentafulvenes, Helvetica chimica acta, **69,** no. 5, (1986), 1052–1064.

[23] Wolfgang Quapp, Michael Hirsch, Dietmar Heidrich, Bifurcation of reaction pathways: the set of valley ridge inflection points of a simple three-dimensional potential energy surface, Theoretical Chemistry Accounts, **100,** no. 5, (1998), 285–299.

[24] Teflah Alresheedi, Ali Allahem, Dynamical study of Lyapunov exponents for Hide's coupled dynamo model, Demonstratio Mathematica, **54,** no. 1, (2021), 189–195.